Reconsider phase reconstruction in chronobiological research from the modern signal processing perspective

Yu-Chen Huang[1], Aymen Alian[2], Yu-Lun Lo[1], Kirk Shelley[2], and Hau-Tieng Wu[3,4]

[1] ***Department of Thoracic Medicine, Chang Gung Memorial Hospital, Chang Gung University, College of Medicine, Linkou, Taiwan***

[2] ***Department of Anesthesiology, Yale University, New Haven, CT, USA***

[3] ***Department of Mathematics and Department of Statistical Science, Duke University, Durham, North Carolina, USA***

[4] ***Mathematics Division, National Center for Theoretical Sciences, Taipei, Taiwan***

Correspondence to

Hau-Tieng Wu, MD. PhD.

Department of Mathematics and Department of Statistical Science, Duke University

120 Science Drive, 117 Physics Building, Campus Box 90320 Durham, NC 27708-0320

Email: haowu@math.duke.edu

Manuscript word count: 6823

Number of figures: 7

Abstract

Background: Phase is the most fundamental physical quantity when we study an oscillatory time series, and there are a lot of tools aiming to estimate phase. Most existing algorithms are developed based on the analytic function model. Unfortunately, this approach might not be suitable for several modern signals, particularly biomedical signals, due to the intrinsic complicated structure, including (possibly) multiple oscillatory components, each with time-varying frequency, amplitude, and non-sinusoidal oscillation. Due to the lack of consensus of model and algorithm, phases estimated from signals simultaneously recorded from different sensors for the same physiological system from the same subject might be different. All these might challenge reproducibility, communication, and scientific interpretation.

Objectives: We need a standardized tool with theoretical supports over a unified model to extract phase.

Methods: We systematically summarize existing models for phase and algorithms and discuss why we may face challenges with them. Then we introduce the *adaptive non-harmonic model (ANHM)* and how to define phase with this model and suggest applying algorithms that can separate oscillatory components and recover their fundamental components, e.g., the *synchrosqueezing transformation (SST)* or the *continuous wavelet transform (CWT)* with a proper time-varying bandpass filter, to extract the phase.

Results: Two databases with different physiological signals, one for respiration and one for hemodynamic, with different clinical applications are explored. We report that the extracted phases following the definition, if properly extracted, are more uniform across different recording modalities and are immune to non-sinusoidal oscillation compared with traditional approaches.

Conclusions: The proposed combination of ANHM and algorithms alleviates the above-mentioned challenges. We expect its scientific impact on a broad range of applications.

Keywords: phase function; wave-shape function; adaptive non-harmonic model; synchrosqueezing transformation; continuous wavelet transform

Introduction

Phase is the most fundamental physical quantity when we study an oscillatory (or periodic) time series. It has been studied over centuries and is a standard material covered in signal processing, communication, physics, and almost all scientific related fields. Roughly speaking, the phase of an oscillatory signal is the relative value of the signal within the span of a single oscillatory period (Figure 1a). It is closely related to the notion of frequency and period. In biomedicine, the phase contains crucial physiological information; for example, the pulse transit time is the phase relationship between electrocardiogram (ECG) and photoplethysmogram (PPG), and it reflects the blood pressure (Gesche 2012; Kim 2013); the coupling between the heart and lung, known as the cardiopulmonary coupling (CPC), is quantified by evaluating the phase relationship of the heart rate and respiration (Schäfer 1999); the coupling between different frequency bands of the electroencephalogram (EEG) or the amplitude-phase coupling (Dvorak 2014; Khodagholy 2017), has been well explored in the neuroscience society (Lachaux 2000; Khodagholy 2017), among others (Rosenblum 2001; Rosenblum 2002), which is far from an exhaustive list.

In a very general sense, the term *phase* describes the status of the system. We may collect all possible statuses of the system and call the collection the *phase space*. The flow-volume loop (Miller 2005) or pressure-volume diagram (Klabunde 2011) are common examples related to phase. In the flow-volume loop, the respiratory dynamics is described by the pressure and volume, which could be understood as "phase". In some applications, when physiological knowledge is sufficient, it is possible to consider modeling the physical dynamical system by a set of equations and hence further describe and estimate the phase space and the phase. There is a huge literature discussing this approach, ranging from the famous Hodgkin-Huxley model (Hodgkin

1952) to many current models like (Wigren 2015; Ashwin 2016), which again is a far from exhaustive list. While such a differential equation approach usually leads to a more interpretable system, this direction, however, is not the focus of this work since a satisfactory model for many biomedical signals is usually lacking. For interested readers, we refer them to, for example, the monograph (Murray 2007; Keener 2009) for more details. In this paper, we focus on the case when the available data is oscillatory time series, and discuss how to define, and then extract, its associated phase function based on a descriptive, or phenomenological, model.

Historically, there has been rich literature discussing the theoretical foundation of phase function, for example (Gabor 1946; Van der Pol 1946; Bedrosian 1962; Rihaczek 1966; Picinbono 1997), which is again far from an exhaustive list. The widely accepted model for the phase function is the analytic function model (Gabor 1946; Nevanlinna 1970; Picinbono 1997) proposed by Gabor back in 1946 (Gabor 1946), based on which most existing theories and phase extraction algorithms are developed. The Hilbert transform (Oppenheim 1999) with or without a bandpass filter design or its variations (Feldman 2006), time frequency (TF) analysis tools like continuous wavelet transform (CWT) (Daubechies 1992) or others (Cohen 1989; Flandrin 1998), Blaschke decomposition (Nahon 2001) or adaptive Fourier transform (Qian 2010), or even empirical mode decomposition (Huang 1998), are commonly applied algorithms to estimate the phase function from an observed signal. This analytic function model and associated algorithms (hereafter called traditional approach) have been successfully applied to various scientific fields, like the communication system or information processing with solid theoretical support. In biomedicine, the traditional approach has usually been the choice (Chavez 2006), and it is claimed in Le Van Quyen M et al (Le

Van Quyen 2001) that there are minor differences between the Hilbert transform and CWT on the intracranial or scalp EEGs.

An ideal definition of phase function should not only be theoretically rigorous, but also properly describe the status of the system with physiological meaning. However, in biomedicine, depending on the signal, the traditional approach might not fulfill these criteria. For example, its application to the respiratory signal, PPG, peripheral venous pressure (PVP) (Wu 2020), etc., might be problematic since they may contain multiple physiological oscillatory components, and each of them oscillates with *non-sinusoidal oscillatory pattern, time-varying frequency and amplitude*. The estimated phase might thus be not physiologically meaningful. See Figure 4(a) for an illustration, where the phase estimated from the end-tidal CO_2 ($EtCO_2$) signal fluctuates fast so that the associated frequency goes beyond 0.8Hz, while the associated $EtCO_2$ signal shown in Figure 2(a) obviously does not oscillate that fast. This leads to a problematic interpretation of what the phase is. Moreover, for the same system, different sensors lead to different oscillatory patterns. See Figure 2(b) for an illustration of four different respiratory signals recorded simultaneously. This diverse oscillatory pattern further impacts the estimated phase if we apply the traditional approach. See Figure 4(a) for an illustration, where the phases estimated from different respiratory signals are different, and hence the associated frequencies. These lead to diverse phase estimates, and hence a lack of consensus of what the phase is.

In this paper, we argue that the traditional approach might not be suitable, and in what sense, for several modern time series, particularly oscillatory biomedical signals. We will also provide a solution to this challenge. To the best of our knowledge, this topic is less systematically discussed in biomedicine, except some reports (Le Van

Quyen 2001). The lack of consensus, or standard, might lead to the challenge of reproducibility, communication, and scientific interpretation.

The paper is organized in the following way. To address a broader audience, we start from layman's language to review how an oscillatory biomedical signal is modeled and what is phase based on the analytic function model. This review leads to the suggested adaptive non-harmonic model (ANHM), which offers a platform to standardize the definition of phase that can be properly interpreted physiologically. We then suggest to estimate our proposed phase by any tools that are capable of decomposing the signal into its oscillatory components, and hence recovering their fundamental components, like the synchrosqueezing transform (SST) (Daubechies 2011; Chen 2014) or CWT (Daubechies 1992) with a proper modification that will be detailed below. We demonstrate how to apply the proposed approach in practice by analyzing two clinical databases and comparing them with the traditional approach.

What is phase? From old to new.

See Figure 1(b) for an illustration of the relationship among these models and definitions.

From harmonic function to generalized harmonic function.

In the textbook setup (Oppenheim 1999) , an oscillatory time series is expressed by the *harmonic function:*

$$F(t) = a_0 e^{i(2\pi\xi_0 t+\varphi_0)}, \qquad (1)$$

where $a_0 > 0$ is the amplitude, $\xi_0 > 0$ is its frequency, and $\varphi_0 \in [0,2\pi]$ is the *global phase shift*. The *phase function* is defined as $2\pi\xi_0 t + \varphi_0$. See Figure 2(a) for an example. Given $\mathrm{F(t)}$, it is transparent to evaluate the phase function directly by

unwrapping the function $\frac{F(t)}{|F(t)|} = e^{i(2\pi\xi_0 t+\varphi_0)}$. Usually, the signal we record is real-valued; that is, the signal is usually of the real part of F(t), and a common practice is applying the Hilbert transform to recover $F(t)$ from its real part, and then get the phase function.

However, most physiological signals are not harmonic since they oscillate with time-varying frequency and amplitude. For example, a subject might breathe at different rates at different moments (Benchetrit 2000). This behavior can be modeled by:

$$F_0(t) = A(t)e^{i2\pi\varphi(t)}, \qquad (2)$$

where $A(t)$ is a smooth positive function and $\varphi(t)$ is a smooth monotonically increasing function. We call $\varphi'(t) > 0$ the *instantaneous frequency* (IF) and $A(t)$ the *amplitude modulation* (AM) of the function $F_0(t)$ (Daubechies 2011). In (2), the phase function we are concerned with in this paper is defined as $\varphi(t)$. See Figure 2(a) for an example. Clearly, (1) is a special case of (3) when both the AM and IF are positive constants, and the phase is a linear function. Physically, at time t, the signal $F_0(t)$ repeats itself in about $1/\varphi'(t)$ seconds with an oscillatory magnitude $A(t)$. This function has been shown to well approximate several physiological signals (LIN, WU et al. 2014, Wu 2020). In this model, since $|F_0(t)| = A(t)$, the phase can be easily uniquely evaluated by unwrapping $\frac{F_0(t)}{|F_0(t)|} = e^{i2\pi\varphi(t)}$.

In practice, the signal is real and satisfies

$$f_0(t) = A(t)\cos(2\pi\varphi(t)), \qquad (3)$$

where the meanings of $\varphi'(t)$, $\varphi(t)$, and $A(t)$ are the same as those in (2). It might be intuitive to define the phase function to be $\varphi(t)$. However, it is not true due to the

identifiability issue. Indeed, it is easy to find infinite pairs of $\tilde{\varphi}(t)$, and $\tilde{A}(t)$ so that $A(t)\cos\big(2\pi\varphi(t)\big) = \tilde{A}(t)\cos\,(2\pi\tilde{\varphi}(t))$ for all time t. Thus, without knowing $A(t)$, the phase cannot be uniquely defined.

Another intuitive approach is considering the Hilbert transform to convert (3) into an analytic function so that the phase can be uniquely defined. However, unlike the relationship between (1) and its real part, we face a challenge in this approach, which is closely related to the *Vakman's problem* (Vakman 1972; Vakman 1996; Huang 2013). Specifically, applying the Hilbert transform to recover $F_0(t)$ from $\mathrm{f}_0(\mathrm{t})$ is not usually mathematically possible since $F_0(t)$ is usually *not* an analytic function, nor a unitary function (Picinbono 1997). As a result, a spectral leakage is inevitable, which could be quantified in the global L^2 sense (Bedrosian 1962; Nuttall 1966). On the other hand, the Hilbert transform cannot recover $F_0(t)$ unless some specific conditions are satisfied (Bedrosian 1962; Nuttall 1966). However, these conditions are limited (Picinbono 1997) and hold only for specific signals, like those considered in communication systems. We shall elaborate that the model is not mathematically correct, it could be *physically accurate* (Picinbono 1997) and hence practically useful. A typical example is the frequency modulation with high carrier frequency in the radar communication. However, for the biomedical time series, this model might also be physically inaccurate since the carrier frequency is usually low compared with the variation of the varying frequency, and hence in general the phase defined under the model (2) cannot be estimated accurately or even correctly interpreted by the Hilbert transform. See Figures 4(a) and 6(a) for examples, and more discussions in the later section.

Despite the above limitations, it has been found that under some reasonable conditions, we can still make sense of the model (3) for the phase definition. A

reasonable condition is the *slowly varying AM and IF* (Daubechies 2011; Chen 2014); that is, the AM and IF change slowly compared with the IF. Mathematically, this assumption is described by

$$|\varphi''(t)| \leq \epsilon\varphi(t) \text{ and } |A'(t)| \leq \epsilon\varphi(t) \qquad (4)$$

for some small $\epsilon > 0$ for all time t. When this condition is satisfied, (3) is called the *intrinsic mode-type* (IMT) function. This model reflects physiological homeostasis – the variability from cycle to cycle does not change dramatically during a short time without external stimulations, while the system might migrate from one status to another over a long period. Under such a condition, it is shown in (Chen 2014) that the identifiability issue is resolved, and the phase can be uniquely defined up to a negligible error. Thus, it does make sense to define the phase to be the same as that in the model (2). Before introducing an alternative algorithm to estimate the phase of an IMT function, we shall discuss a more realistic model.

More realistic model – multiple components with wave-shape function

There are more detailed features that cannot be captured by the IMT function. One feature is the *non-sinusoidal* oscillatory pattern. For example, ECG or PPG do not oscillate like a sine wave. Moreover, usually a biomedical signal is composed of several components with different physiological interpretations. For example, the PPG signal is composed of one hemodynamic component and one respiratory component known as the respiratory induced intensity variation (RIIV) (Shelley 2007); the respiratory signal is composed of one respiratory component, and one hemodynamic component known as the cardiogenic artifact (Luo 1994). This fact holds for other biomedical signals. These observations lead to the ANHM: (Wu 2013; Lin 2018)

Definition 1 [Adaptive non-harmonic model]. A function $f(t)$ satisfies the ANHM if it has the expression

$$f(t) = \sum_{l=1}^{L} f_l(t), \qquad (5)$$

where $L \geq 1$, and for each $l = 1, \dots, L$,

$$f_l(t) = A_l(t) s_l(\varphi_l(t)), \qquad (6)$$

where $A_l(t)$ and $\varphi_l(t)$ have the same meanings as those in (3) and satisfy (4), and s_l is a real 1-periodic function with the unit norm. We call $f_l(t)$ the l-th non-harmonic IMT function of the signal $f(t)$, and $s_l(t)$ the wave-shape function (WSF) of the l-th oscillatory component.

See Figure 2(a) for a simulated example with a non-sinusoidal oscillatory signal when $L = 1$, and Figures 2(b) and 2(c) for several real physiological signals. Clearly, (5) is a generalization of (3) since when $L = 1$ and $s_l(t) = \cos(2\pi t)$, (5) is reduced to (3). This ANHM will be our base to propose a standardized definition of phase for a biomedical signal. Since our focus is the phase, we simplify the discussion without adding noise in (5), and refer readers to (Chen 2014; Sourisseau 2019) for the noisy cases. In practice, L in (5) is known based on our physiological knowledge. See Discussion for more discussion about L. We shall mention that there have been several generalizations, e.g. the time-varying WSF (Lin Su 2018) and wave-shape manifold (Lin Malik 2019), to better capture the biomedical signals (see more in (Wu 2020)). To simplify the discussion, we focus on Definition 1.

<u>*When* $L = 1$</u>. Note that $s(\varphi(t))$ in $f(t) = f_1(t) = A(t)s(\varphi(t))$is nothing but "stretching" $s(t)$ by $\varphi(t)$, and then "scaling" by $A(t)$. We thus have the following definition:

Definition 2 [Standardized phase when $L = 1$*]. The phase function of* $f(t)$ *satisfying (5) with* $L = 1$ *is* $\varphi(t)$.

We need to mention a critical possible confusion point here. When the Hilbert transform is applied to $f(t)$, f(t) can be written as the real part of $\tilde{a}(t)e^{i2\pi\tilde{\varphi}(t)}$, where if we enforced $\tilde{a}(t) > 0$, $\tilde{\varphi}(t)$ might *not* be a monotonic increasing function. In the traditional approach, the widely accepted definition of phase function of f(t) as $\tilde{\varphi}(t)$, and hence the declared IF might be negative, which might be challenging to interpret. See a simulation in Figure 3 as an example of such a model and approach. Even worse, this approach is sensitive to the input signal, even if two signals shown in Figure 3 are "visually similar". This fact comes from the "winding" effect from the complex analysis perspective.

To look deeper into ANHM, consider a different interpretation of the signal $f(t) = f_1(t) = A(t)s(\varphi(t))$. To simply the discussion, suppose $s(t)$ is sufficiently smooth with mean 0, so (5) could be expanded by the Fourier series point wisely as

$$f(t) = A(t)\sum_{k=1}^{\infty} a_k \cos(2\pi k\varphi(t) + b_k), \qquad (7)$$

where we assume $a_1 > 0$, and set $a_k \geq 0$ for $k > 1$, $b_k \in 0,2\pi]$, and $\sum_{k=1}^{\infty} a_k^2 = 1$. The interpretation of $f(t)$ in (7) is different – $f(t)$ is composed of multiple *sinusoidal* oscillatory components. We call $a_1 cos(2\pi\varphi(t) + b_1)$ the *fundamental component* and $a_k cos(2\pi\varphi(t) + b_k)$, $k > 1$, the $(k-1)$-*th multiple* of the fundamental component. Clearly, the phase function we consider, $\varphi(t)$, is the phase function of the fundamental

component, while the phase in the traditional approach, $\tilde{\varphi}(t)$, contains information not only from the fundamental component, but also from *all* multiples. As a result, sometimes researchers apply a BPF or CWT to eliminate the impact of multiples. However, due to the time-varying frequency and amplitude, this spectral information of multiples might leak and contaminate the result. In short, while the model (5) could model various physiological time series, the traditional approach might not work as expected.

Now, we argue why it is better to define the phase to be $\varphi(t)$ instead of $\tilde{\varphi}(t)$ by taking physiological knowledge into account. Take ECG as an example (see Figure 1(a)), where the IF, AM and the WSF have their own physiological meanings. The WSF of ECG reflects the electrical pathway inside the heart, where the sensor is put, the heart anatomy, etc. Several clinical diseases are diagnosed by reading the WSF but not reading its Fourier decomposition in (7). Moreover, while time moves forward, the physiological status should "move forward"; that is, the phase function should be monotonically increasing. This physiological fact suggests that it is better to separate the WSF from the phase function as in (6), which is precisely our definition of the phase function when $L = 1$. See Section 4 for concrete examples, like that in Figure 4(a).

Our definition has more benefits from the perspective of IF and AM. In the ECG example, it is well known that while the rate of the pacemaker is constant, the heart rate generally is not constant. The discrepancy comes from neural and neuro-chemical influences on the pathway from the pacemaker to the ventricle. This non-constant heartbeat rate could be modeled as the IF of the ECG. Moreover, the AM of the ECG reflects the breathing activity via the thoracic impedance. If we take model (7) into account, the interpretation of IF and AM might not be physiological.

In summary, we advocate that a phase function $\varphi(t)$ shall describe at which status the oscillation is at each time, and the status is described by the WSF. On the other hand, the phase function $\widetilde{\varphi}(t)$ is a mix-up of this status information and the WSF, and an interpretation of $\widetilde{\varphi}(t)$ is usually challenging.

<u>*When $L > 1$*</u>. In this case, we may again try to define the phase function via the Hilbert transform, which we also denote $\widetilde{\varphi}(t)$. When $L > 1$, we may again have an interpretation problem even if $s_l(t) = \cos(2\pi t)$ for $l = 1, \dots, L$ since the phase information of different oscillatory components might be mixed-up. This leads to the same problem shown in Figure 3 discussed above, since (5) with $L = 1$ is a special case when $L > 1$ and $s_l(t) = \cos(2\pi t)$ for $l = 1, \dots, L$. Moreover, when $L > 1$, the phase of each non-harmonic IMT function shall have its own meaning. Take PPG as an example. Since PPG is composed of a respiratory component and a cardiac component, which obviously have different physiological contents, one phase $\widetilde{\varphi}(t)$ might not fully capture the complicated physiology underlying PPG. To resolve this issue, we propose to define the phase of (5) to be a *collection* of phase function associated with each oscillatory component:

Definition 3 [Standardized phase when $L > 1$]. The phase function of $f(t)$ satisfying (5) when $L > 1$ is a set of phase functions $\{\varphi_1(t), \dots, \varphi_L(t)\}$, or equivalently a vector valued function $\Phi(t) = [\varphi_1(t), \dots, \varphi_L(t)]^T$ when $t \in \mathbb{R}$.

Note that Definition 2 is a special case of the standardized phase in Definition 3. Take PPG as an example again. The "phase" as a set of functions, or a vector-valued function, jointly describe the physiological dynamics of different systems at each time. In summary, we propose to use ANHM in Definition 1 to describe various oscillatory

physiological signals, and the associated phase function can be standardized and defined unambiguously with physiological meanings in Definitions 2 and 3.

Methodology

We introduce methods to estimate the proposed phase, including CWT (Daubechies 1992) and SST (Daubechies 2011). We mention that any tools that can separate and reconstruct the fundamental component of each non-harmonic IMT function could be used to estimate the standardized phase, while we only discuss CWT and SST to avoid distracting the readers. The key idea is applying a *time-varying bandpass filter (tvBPF)* where the spectral band depends on time. This is possible by taking the strength of TF analysis into account. In contrast, traditional approach usually depends on the bandpass filter (BPF) with a fixed spectral band, even if CWT or other TF analyses tools are applied. The code and data for regenerating the results in Section 4 can be found in https://www.dropbox.com/sh/hjanz99ho7rjxim/AAA8kbATMmm34aDqOkhD8jI6a?dl=0

Recall TF analysis tools—CWT and SST

Fix the Gaussian function $h(t) = e^{-t^2}$. While the window can be more general, we focus on the Gaussian function to simplify the discussion. Take the signal f, and assume it is a tempered distribution. The short time Fourier transform (STFT) (Cohen 1989, Flandrin 1998) of f is defined as

$$V^{(h)}(x,\xi) = \int f(t)h(t-x)e^{-i2\pi t\xi}dt, \qquad (8)$$

where $x \in \mathbb{R}$ means time and $\xi > 0$ means frequency. We call the set of pairs(x, ξ) the TF domain, and $V^{(h)}$ is the TF representation (TFR) of $f(t)$ via STFT. Call $\left|V^{(h)}\right|^2$ the *spectrogram*.

CWT is different from STFT while share several similarities. Consider an analytic mother wavelet ψ, which has mean zero and unit norm, and assumed to have sufficient smoothness and integrability to simplify the discussion, the CWT of $f(t)$ is defined as

$$C^{(h)}(a, b) = \int f(t) \frac{1}{\sqrt{a}} \psi\left(\frac{t-b}{a}\right) dt, \qquad (9)$$

where $b \in \mathbb{R}$ means time and $a > 0$ means the scale. Call $\left|C^{(h)}\right|^2$ the *scalogram.* Note that ψ has mean 0 and unit norm, so it is oscillatory. But stretching ψ by a, we could "fit" the signal and detect how fast the signal oscillates. The scale a captures the inverse of frequency (with a proper constant). This is different from STFT, where the signal is truncated by a fixed window, and the Fourier transform is applied. See (Cohen 1989; Flandrin 1998) for a detail treatment of the difference.

SST can be defined on STFT (Wu 2011) and CWT (Daubechies 1992). To demonstrate the idea, we only discuss SST defined on STFT. Note that for each (x, ξ), $V^{(h)}(x, \xi)$ is a complex value, and its *angle* contains useful information that leads to SST. Define the *reassignment rule* as

$$\Omega^{(h)}(x, \xi) = \frac{1}{i2\pi} \frac{\partial_x V^{(h)}(x,\xi)}{V^{(h)}(x,\xi)} \qquad (10)$$

when $V^{(h)}(x, \xi)$ is nonzero and $-\infty$ otherwise. With the reassignment rule, the SST of f is defined by reallocating STFT coefficients by

$$S^{(h)}(x, \eta) = \int_0^\infty V^{(h)}(x, \xi) \delta_{|\eta - \Omega^{(h)}(x,\xi)|}(\xi) d\xi, \qquad (11)$$

where $\eta > 0$ is the frequency and δ denotes the Dirac measure supported at 0. Compared with the STFT, the main benefit of SST is enhancing the contrast of the TFR

determined by STFT by sharpening the spectrogram and hence alleviate the possible spectral mix-up between different components. We may call $\left|S^{(h)}\right|^2$ the *time-varying power spectrum* since it provides momentary spectral information.

The key idea beyond SST is that the reassignment rule tells us how fast the signal oscillates at each time. Indeed, for a given pair of x and ξ, if we rewrite $V^{(h)}(x,\xi) = |V^{(h)}(x,\xi)|e^{i\Phi^{(h)}(x,\xi)}$, where $\Phi^{(h)}(x,\xi) \in [0,2\pi]$, and assume that $\left|V^{(h)}(x,\xi)\right| > 0$, we have $log\left(V^{(h)}(x,\xi)\right) = log\left(\left|V^{(h)}(x,\xi)\right|\right) + i\Phi^{(h)}(x,\xi)$. Since $\frac{\partial_x V^{(h)}(x,\xi)}{V^{(h)}(x,\xi)} = \partial_x log\ (V^{(h)}\ (x,\xi))$ and $\Phi^{(h)}(x,\xi)$ encodes "how fast" the signal oscillated at time x, when the magnitude $log\left(\left|V^{(h)}(x,\xi)\right|\right)$ does not vary too fast, the reassignment rule gives us the information about how fast the signal oscillates at time x. Thus, the squeezing step (11) sharpens the TFR. For readers with interest in theoretical results and statistical inference by SST, we refer them to (Daubechies 2011; Chen 2014; Sourisseau 2019).

Numerical implementation

Suppose the signal $f(t)$ is sampled N times uniformly with the period $\Delta t > 0$; that is, the i-th sample is $f(i\Delta t)$. The CWT implementation is standard, and we refer readers to, e.g., https://statweb.stanford.edu/~wavelab/ and http://tftb.nongnu.org . On the other hand, SST is implemented by discretizing (8), (10) and (11) directly. In (8) and (10), the frequency axis is sampled from $-1/(2\Delta t)$ to $1/(2\Delta t)$ with the resolution $\Delta\xi = 1/(N\Delta t)$ following the Nyquist rate rule. In (11), the frequency axis η is sampled from $1/(N\Delta t)$ to $1/(2\Delta t)$ with the resolution $1/(N\Delta t)$. But in practice, we may choose a coarser grid (a lower resolution) to speed up the computational time; that is, the

frequency axis η is sampled from $\Delta\eta$ to $m\Delta\eta$, where $\Delta\eta > 0$ is the resolution and $m \in \mathbb{N}$ satisfying $m\Delta\eta = 1/(2\Delta t)$. Denote the discretized TFR $S^{(h)}$ as a $N \times m$ matrix $\boldsymbol{S}$.

Obtain the standardized phase by time-varying BPF

The tvBPF is composed of three steps, which are common for CWT and SST. We explain it with SST. We start from $L = 1$. First, we estimate the IF of the fundamental component by the ridge extraction [23]:

$$c^* = \max_{c \in Z_m^N} \sum_{n=1}^{N} log \left[\frac{|\boldsymbol{S}(c(n),n)|}{\sum_{i=1}^{m}\sum_{j=1}^{N}|\boldsymbol{S}(j,i)|}\right] - \lambda \sum_{n=2}^{N} |c(n) - c(n-1)|^2, \qquad (12)$$

where $\lambda > 0$ is a parameter chosen by the user and $Z_m = \{1,2,\dots,m\}$. Clearly, c is a N-dim vector. The first term in (12) means we fit a curve c to the TFR $\boldsymbol{S}$ so that the curve captures the most intense pixels in the TFR, while the second term imposes the smoothness constraint on the curve c. By balancing between these two terms, c^* represents a smooth curve on the TFR that captures the IF of the fundamental component. In this work, we choose λ=0.5. According to the established theory (Daubechies 2011; Chen 2014), the IF of the fundamental component at time $i\Delta t$ is $c^*(i)\Delta\eta$. Second, we reconstruct the fundamental component from $\boldsymbol{S}$ via

$$\tilde{f}(i\Delta t) = \Delta\eta \sum_{j=c^*(i)-D}^{c^*(i)+D} \boldsymbol{S}(i,j), \qquad (13)$$

where $D \in \mathbb{N}$ is chosen by the user. That is, at time $i\Delta t$, we sum up the frequency band centered at the IF $c^*(i)\Delta\xi$, with the bandwidth $D\Delta\eta$. See Figure 5(a) for an illustration, where the dashed curves below and above the solid red curve indicates the band, while the solid red curve indicates the extracted ridge. Combining (12) and (13) is the tvBPF. In practice, $D\Delta\eta$ is suggested to be about 1/10 of the fundamental frequency. In this work, we choose D so that $D\Delta\eta = 0.1$. According to the established theory (Wu 2011), $\tilde{f}$ well approximates the complex form of the fundamental component of the

oscillation ingredient we have interest; that is, for $f(t) = f_1(t) = A(t)s(\varphi(t))$, we have $\tilde{f}(i\Delta t) = A(i\Delta t)a_1 e^{i(2\pi\varphi(i\Delta t)+b_1)}$ up to a negligible error. Third, according to (6), since $A(i\Delta t)a_1$ is not zero, the standardized phase at time $i\Delta t$ can be estimated by unwrapping $\tilde{f}(i\Delta t)/|\tilde{f}(i\Delta t)|$.

When $L > 1$ in (5), the standardized phase is obtained by iterating the above three steps with an extra step. Specifically, after obtaining the standardized phase of the first non-harmonic IMT function, mask the curve and its multiples associated with the first non-harmonic function in the TFR; for example, set $\boldsymbol{S}(kc^*(i), i)$ to be $\boldsymbol{S}(kc^*(i), i)/10$ for $i = 1, \ldots, N$ and $k = 1, \ldots, \lfloor m/c^*(i) \rfloor$, to suppress the impact of the first non-harmonic IMT function. Then, apply (12) again to find the fundamental frequency of the second non-harmonic IMT function, and so on. By iteration, we obtain the standardized phase of the signal $f(t)$.

In Figure 3, we illustrate the estimated phase of a simulated chirp signal with non-sinusoidal oscillation. Clearly, the trouble we encountered by the Hilbert transform is eliminated. As we will show below in the real data, even if the IFs of different components have separate ranges, it is not always a good idea to apply the traditional approach, when the signal oscillates with IF and AM.

Material and methods

We consider two databases to demonstrate how to apply the proposed standardization and tools.

First database—COPD

The first database comes from a prospective study that recruits patients with a clinical diagnosis chronic pulmonary obstructive disease (COPD) according to the Global Initiative for Obstructive Lung Disease Criteria at Chang Gung Memorial

Hospital (CGMH), Linkou, Taiwan, from January 2019 to December 2019. The ethics committee of CGMH approved the study. All participants signed informed consent before enrollment. Patients with heart failure (Ejection fraction <40%), lung cancer, atrial fibrillation, using anti-arrhythmic agents and using oxygen were excluded. Total of 63 patients were included, with impaired pulmonary function tests with FVC (Forced vital capacity) 79% (42%-130%) and FEV_1 (Forced expiratory volume in the 1st second) 58% (21-105%). Experiments were carried out in a quiet room with the temperature maintained at 22-24 ^{o}C. Patients were instructed to avoid bronchodilators such as beta-2 agonists, xanthene derivatives, alcohol, and coffee before the experimental test. Before the examination, blood pressure, heart rate, and oxygen saturation were recorded. They wore the pulse oximeter on the finger and ECG electrodes on the chest wall. We recorded the flow signal, impedance, and end-tidal CO_2 ($ETCO_2$) for 5 minutes continuously. To avoid any signal quality issue, the skin was abraded with gel then cleaned with alcohol to reduce skin electrode impedance before ECG electrodes attached, and before the recording, the patient practiced breathing via the flow tube for 45 seconds. Three Actiwave devices were used for recording flow signals and ECG signals. Recording signals were transferred via European Data Format to LabChart 8 analysis software (ADInstruments, USA), and then exported to text files for analysis. The goal is to compare different methods to estimate the phase of the respiratory component, and hence the cardiopulmonary coupling (CPC), from various respiratory sensors.

Second database--LBNP

The second database comes from a previous prospective study that recruits normal subjects for the lower body negative pressure (LBNP) experiment that simulates

blood loss. After approval of the protocol by the Yale University Human Committee, healthy subjects of both sexes with age 18-40 years were recruited and provided written consent. Exclusion criteria were current pregnancy or any history of pulmonary, cardiac, or vascular disease including hypertension effectively treated with antihypertensive medication. Subjects were instructed to refrain from alcoholic and caffeinated beverages, strenuous exercise, and tobacco consumption for at least 12 hours prior to the study. A negative pregnancy test was confirmed for all female subjects immediately before participation. Intravenous access was established as a precautionary measure, but fluids were not infused during the study. Thirty-five cases remain in the final analysis. Each subject was monitored with various channels, but we only focused on ECG, finger PPG and PVP (Nonin Medical, Inc., Plymouth, MN). Each procedure was performed in a climate-controlled laboratory at 72°F and 20% humidity. Details of the LBNP experiment are well described (Alian 2011). Briefly, after the leg raising test and following a subsequent 5-minute equilibration period, the chamber was sealed to start the LBNP. This entailed 3 minutes phases during which the pressure was progressively decreased by 15 mmHg until either 3 minutes at -75 mmHg were completed or at any phase symptoms consistent with significant hypovolemia occurred. Once an endpoint was reached, pressure in the chamber was increased to -30 mmHg for 1 minute then to 0 for 3 minutes before concluding the study. The goal is to compare different methods to estimate the phase of the hemodynamic component, and hence the instantaneous heart rate (IHR), from PPG and PVP when the hemodynamic is perturbed during the LBNP experiment.

Statistics

For the first database, the agreement of estimated phases is evaluated by two different approaches. The first one is evaluating the agreement of respiratory phases determined from different sensors. The phase difference is quantified, and for each subject the mean and standard deviation are recorded. Results of all subjects are presented as mean±standard deviation. The Mann-Whitney Wilcoxon test is applied to evaluate differences of two variables. P-value less than 0.05 is considered statistically significant. The second one is showing how the phase estimation algorithm influences the widely used algorithm called synchrogram proposed in (Schäfer 1998) to quantify CRC (Pikovsky 1997; Rosenblum 2002). It has been shown in (Huang 2021) that CRC encodes rich clinical information about COPD patients. The synchrogram is composed of two steps. First, for each subject, determine IHR by the standard cubic spline interpolation of R peak to R peak interval (RRI) time series, where the impact of ventricular premature contraction is modified by the standard RRI correction algorithm (Peltola 2012). Then, for each subject, quantify the phase lock of the IHR and respiration by the stroboscope idea, which leads to the synchrogram index. The BA plot is applied to evaluate the limit of agreement (LoA) of the synchrogram indices evaluated from different respiratory sensors over the 63 subjects. The bias, LoA, and the associated 95% confidence interval (CI) are reported for each pair of sensors.

For the second database, we evaluate how the phase of the hemodynamic component, and the associated IHR, could be accurately estimated and the result is independent of the sensor by the proposed standardized phase and tool. The ground truth IHR is determined by the same method used in the first database, which is sampled at 4Hz. For each subject, the median of the difference of IHR determined by PPG or PVP sampled at 4Hz and the ground truth IHR is recorded and the mean and standard deviation of the median difference by different sensors of all subjects are reported. The

Wilcoxon rank test is applied to evaluate if the accuracy of evaluating IHR by different methods is similar, where $p<0.05$ is considered statistically significant. The BA plot is applied to evaluate the consistency of different sensors, and the same summary statistics as those in the first database are reported.

Results

First database—COPD

Besides the proposed tvBPF, we also apply the traditional approach, including the Hilbert transform following a BPF (BPF-HT) and the CWT with a fixed spectral band (CWT-fixed) to estimate the respiratory phase from each respiratory sensor. See Figure 5(b) for an illustration of CWT-fixed applied to different respiratory sensors. In both BPF-HT and CWT-fixed, we consider the spectral band [0.1,0.4] Hz that covers the usual respiratory rate range. We also consider the Blaschke decomposition (BKD) approach, another theoretically solid approach that adaptively decomposes the signal into its components for phase evaluation (see (Coifman 2017) for details).

See Figure 2(b). Those signals have different WSFs, but the length of respiratory cycles is similar since they capture the same physiological system. If this polymorphic behavior of respiratory signals is not properly handled, the phase information might be contaminated. In Figure 4(a), we show that by BPF-HT, the phases of all signals "look close" but the IFs, the derivative of the phase, of all channels are different and not physiologically sensible (CWT-fixed result is the same and depicted in Figure 5(d)). This shows the problem of applying the traditional approach. The TFRs of those signals by SST are shown in Figure 4(b), where we see a clear and dominant curve around 0.5Hz in each TFR, which means that the IFs of all signals' fundamental components are consistent. The estimated phases and their derivatives are also consistent among all

channels, which are shown in Figure 4(c). Compared with Figure 4(a), the results by SST are more sensible and consistent. The results by CWT-tvBPF are similar but not shown here (See Figure 5(b) for an example).

In Figure 5(c-e), a further comparison of respiratory phase determined from different respiratory signals and different methods is shown. The estimated fundamental components and the associated phase (shown in Figure 5(c-d) with the phase mod π) by the BPF-HT, BKD and CWT-fixed visually look different among different sensors, while those estimated by the tvBPF approach, including SST and CWT, are similar, except a global phase shift among sensors. Physiologically, this global phase shift describes the intrinsic difference among different respiratory sensors. The phase discrepancy between two sensors is shown in Figure (d-e), where the discrepancy fluctuates more in Figure (d). This indicates that the phase estimated by CWT-fixed is not consistent if a different sensor is used.

In Table 1, we report the agreement of phase estimation from different pairs of respiratory sensors and methods. It suggests that the global phase difference between two sensors is usually consistent among different methods. However, the standard deviation is statistically smaller if SST or CWT-tvBPF is applied. The performances of BKD and CWT-fixed are similar. This is because BKD is sensitive to the non-sinusoidal oscillation.

To further demonstrate its clinical application, the CRC indices of 63 subjects determined by the synchrogram from different respiratory signals are compared by the Bland-Altman plot. The bias, LoA, and the associated 95% CI are reported for each pair of sensors in Figure 6. The results suggest that if the respiratory phase is estimated by the tvBPF, either SST or CWT, the CRC index is less impacted by the sensor type compared with other methods.

Second database--LBNP

Two segments of PPG and PVP simultaneously recorded from a healthy subject during the baseline and during the -75mmHg pressure (simulating a 1,500cc blood loss) are shown in Figure 2(c). For a single subject, the WSFs of PPG and PVP are different in different physiological status. Based on the COPD result, we only compare BPF-HT and SST. In Figure 7(a), we show the estimated phases by BPF-HT with different spectral bands, and both are not sensible.

See Figure 7(b) for the TFRs of PPG and PVP by SST. In both TFRs, there is a dominant curve starting at around 1.8Hz, surging to 2.5Hz in the 4/5 of the experiment (around -75mmHg), and then coming back to 2Hz. This reflects the fact that during a massive blood loss, tachycardia happens. The multiple can also be clearly seen. There are more structures in the TFR of PVP, like a dominant curve at 0.3Hz, and a vague curve around 1Hz from 600sec to 1100sec. The curve at 0.3Hz is associated with the respiration, and the curve around 1Hz from 600sec to 1100sec is unknown to our knowledge and needs more exploration. These indicate that there are multiple non-harmonic IMFs constituting PVP. In Figure 7(c), the proposed tvBPF successfully gives a sensible phase of the cardiac component, and hence the IHR via differentiation. Since both PPG and PVP reflect the cardiac cycles, it makes sense that the estimated IHRs are close. However, the IHR estimated from PVP is noisy. It is not surprising since PVP is usually noisy.

Quantitatively, among all subjects, the median IHR estimation errors from PPG and PVP by SST are 0.0007±0.0004 Hz and 0.0077±0.0049 Hz respectively, while the median IHR estimation errors from PPG and PVE by BPF-HT are 1.18±0.185 Hz and 1.165±0.176 Hz respectively. The p-value of the Wilcoxon test comparing the

performance of BPF-HT and SST of estimating the IHR from PPG and PVP are $<10^{-4}$ and $<10^{-4}$ respectively, which are both statistically significant after the Bonferroni correction. The agreement bias of estimating the IHR from PPG and PVP by SST and BPF-HT are 0.006 and -0.019 respectively, with the upper LoA 1.34 [95% CI: [1.33, 1.34]] and 0.042 [95% CI: [0.041, 0.042]], and the lower LoA -1.32 [95% CI: [-1.32, -1.33]] and -0.081 [95% CI: [-0.080, -0.081]] respectively. The above results indicate that SST could estimate IHR more accurately compared with BPF-HT from both PPG and PVP.

Discussion

Phase is a fundamental quantity describing an oscillatory signal. We show that the phase coming from the analytic function model and traditional approach might not be suitable for biomedical signal analysis. We then suggest standardizing the phase definition by modeling oscillatory biomedical time series by ANHM and consider the standardized phase. Then, we suggest applying tvBPF with, e.g., SST and CWT, to extract the standardized phase. We demonstrate the procedure by analyzing two databases, and show that the proposed phase, when combined with a proper algorithm, is less independent of the sensor type. We also provide a Matlab implementation for researchers.

This result is critical in the heterogeneous clinical environment, which becomes more diverse in the post-COVID 19 era. In digital medicine, different respiratory sensors are available to acquire respiratory information, while they differ from different perspectives, like signal quality, ease-of-use and what information could be acquired. For example, a continuous recording of flow signals is less suitable for home-based healthcare, however it provides more information. On the other hand, the impedance

respiratory signal could be easily acquired, but the quality is less stable and less information, like tidal volume, could be directly obtained. Without a standardized approach, it would be challenging to exchange information if different respiratory sensors are used, and an advance of scientific knowledge could be limited. We would expect that if this standardized phase is properly used, it helps scientific research from different aspects, including information sharing, discussion of the scientific findings among different equipment, and others.

To achieve a fully automatic estimation of the standardized phase, there are several challenges we shall resolve. First, Definition 1 does not capture more complicated dynamics; for example, the wax-and-wane pattern that an oscillatory component might only appear in a subinterval but not the whole recorded signal. For example, the respiratory component in PPG might exist for a while and disappear over another period. How to automatically determine when a non-harmonic IMT function exists could be framed as a change point problem. While some work has been developed recently, more work is needed. Note that to avoid complications and focus on the notion of standardized phase, we focus on (5) in this paper.

Second, note that Definition 1 might not be applied to properly model some stochastic-process-like physiological signals, like R peak to R peak interval time series, EEG or local field potential, but how well it performs depends on the situation. Take EEG as an example. It is a common practice to find the phase of the alpha band (or other bands) and discuss how it changes or is coupled with other bands according to time. A systematic discussion of the phase of these stochastic-process-like signals under different situations, particularly when Definition 1 is not suitable, shall be further explored.

Third, the ridge extraction algorithm (12) might not be the optimal solution to extract IF, particularly when the multiples have stronger strength, or even when the fundamental component does not exist. The solution is combining rectification and the de-shape algorithm (Lin 2018) Since the focus of this paper is phase, it is not extensively discussed and we refer readers with interest in this solution to (Lin 2018). Fourth, in practice we may or may not know L in (5). Usually, we have physiological knowledge guiding us about L, but when we do not have sufficient knowledge, estimating L from the function $f(t)$ is important. While we could apply the de-shape algorithm (Lin 2018) or follow the iterative approach, providing a systematic approach with confidence is so far a challenging problem. Tackling the above problems will be our future work.

Conclusions

The proposed combination of ANHM and tvBPF with TF analysis tools alleviates the challenges of nonuniform phase extraction across different recording modalities. Under the existing theoretical supports, we expect its scientific impact on a broad range of applications.

Acknowledgements

We thank the investigators and members of the Department of Thoracic Medicine and Anaesthesiology for their efforts.

Financial disclosure statement

This work was not supported by any grant. The funding bodies played no role in the design of the study; the collection, analysis, or interpretation of data; or the preparation of the manuscript.

Availability of data and materials

The data sets analysed during the current study are available from https://www.dropbox.com/sh/hjanz99ho7rjxim/AAA8kbATMmm34aDqOkhD8jI6a?dl=0

Competing interests

All authors declare that they have no competing interests.

References:

1. AA Alian, NJ Galante, NS Stachenfeld, DG Silverman, KH Shelley. 2011. Impact of central hypovolemia on photoplethysmographic waveform parameters in healthy volunteers part 2: frequency domain analysis. Journal of clinical monitoring and computing. 25(6): 387-396.
2. P Ashwin, S Coombes, R Nicks. 2016. Mathematical frameworks for oscillatory network dynamics in neuroscience. The Journal of Mathematical Neuroscience. 6 (1): 1-92.
3. E Bedrosian. 1962. A product theorem for Hilbert transforms.
4. G Benchetrit. 2000. Breathing pattern in humans: diversity and individuality. Respiration physiology. 122 (2-3): 123-129.
5. M Chavez, M Besserve, C Adam and J Martinerie. 2006. Towards a proper estimation of phase synchronization from time series. Journal of Neuroscience methods. 154 (1-2): 149-160.
6. YC Chen, MY Cheng, HT Wu. 2014. Non-parametric and adaptive modelling of dynamic periodicity and trend with heteroscedastic and dependent errors. Journal of the Royal Statistical Society: Series B: Statistical Methodology. 651-682.
7. L Cohen. 1989. Time-frequency distributions-a review. Proceedings of the IEEE. **77**(7): 941-981.
8. RR Coifman, S Steinerberger, HT Wu. 2017. Carrier frequencies, holomorphy, and unwinding. SIAM Journal on Mathematical Analysis. 49 (6): 4838-4864.
9. I Daubechies. 1992. Ten lectures on wavelets. SIAM, Philadelphia, 1992. MR 93e 42045.
10. I Daubechies, J Lu, HT Wu. 2011. Synchrosqueezed wavelet transforms: An empirical mode decomposition-like tool. Applied and computational harmonic analysis. **30** (2): 243-261.
11. D Dvorak, AA Fenton. 2014. Toward a proper estimation of phase–amplitude coupling in neural oscillations. Journal of Neuroscience methods. 225: 42-56.
12. M Feldman M. 2006. Time-varying vibration decomposition and analysis based on the Hilbert transform. Journal of Sound and Vibration 295 (3-5): 518-530.
13. P Flandrin. 1998. Time-frequency/time-scale analysis. Academic press.
14. D Gabor. 1946. Theory of communication. Part 1: The analysis of information. Journal of the Institution of Electrical Engineers-Part III: Radio and Communication Engineering. 93 (26): 429-441.
15. H Gesche, D Grosskurth, G Küchler, A Patzak. 2012. Continuous blood pressure measurement by using the pulse transit time: comparison to a cuff-based method. European journal of applied physiology 112 (1): 309-315.
16. AL Hodgkin, AF Huxley. 1952. A quantitative description of membrane current and its application to conduction and excitation in nerve. The Journal of physiology. 117 (4): 500-544.
17. J Huang, Y Wang, L Yang. 2013. Vakman's problem and the extension of Hilbert transform. Applied and computational harmonic analysis. 34 (2): 308-316.
18. NE Huang, Z Shen, SR Long, MC Wu, HH Shih, Q Zheng, NC Yen, CC Tung, HH Liu. 1998. The empirical mode decomposition and the Hilbert spectrum for nonlinear and non-stationary time series analysis. Proceedings of the Royal Society of London. Series A: mathematical, physical and engineering sciences. 454 (1971): 903-995.
19. YC Huang, TY Lin, HT Wu, PJ Chang, CY Lo, TY Wang, CH Kuo, SM Lin, FT Chung, HC Lin. 2021. Cardiorespiratory coupling is associated with exercise capacity in

patients with chronic obstructive pulmonary disease. BMC Pulmonary Medicine 21 (1): 1-10.
20. J Keener, J Sneyd. 2009. Mathematical physiology 1: Cellular physiology, Springer.
21. D Khodagholy, JN Gelinas, G Buzsáki. 2017. Learning-enhanced coupling between ripple oscillations in association cortices and hippocampus. Science. 358 (6361): 369-372.
22. SH Kim, JG Song, JH Park, JW Kim, YS Park, GS Hwang. 2013. Beat-to-beat tracking of systolic blood pressure using noninvasive pulse transit time during anesthesia induction in hypertensive patients. Anesthesia & Analgesia. 116(1): 94-100.
23. R Klabunde. 2011. Cardiovascular physiology concepts. Lippincott Williams & Wilkins.
24. JP Lachaux, E Rodriguez, J Martinerie, C Adam, D Hasboun, FJ Varela. 2000. A quantitative study of gamma-band activity in human intracranial recordings triggered by visual stimuli. European Journal of Neuroscience. 12 (7): 2608-2622.
25. M Le Van Quyen, J Foucher, JP Lachaux, E Rodriguez, A Lutz, J Martinerie, FJ Varela. 2001. Comparison of Hilbert transform and wavelet methods for the analysis of neuronal synchrony. Journal of neuroscience methods. 111 (2): 83-98.
26. CY Lin, L Su, HT Wu. 2018. Wave-shape function analysis. Journal of Fourier Analysis and Applications. 24 (2): 451-505.
27. YT Lin, J Malik. HT Wu. 2019. Wave-shape oscillatory model for nonstationary periodic time series analysis. arXiv e-prints: arXiv: 1907.00502.
28. YT Lin, HT Wu, J Tsao, HW Yien, SS Hseu. 2014. Time-varying spectral analysis revealing differential effects of sevoflurane anaesthesia: non-rhythmic-to-rhythmic ratio. Acta Anaesthesiologica Scandinavica. 58(2): 157-167.
29. S Luo, WJ Tompkins, JG Webster. 1994. Cardiogenic artifact cancellation in apnea monitoring. Proceedings of 16th Annual International Conference of the IEEE Engineering in Medicine and Biology Society. IEEE.
30. MR Miller, J Hankinson, V Brusasco, F Burgos, R Casaburi, A Coates, R Crapo, P Enright, C Van Der Grinten, P Gustafsson. 2005. Standardisation of spirometry. European respiratory journal. 26 (2): 319-338.
31. JD Murray. 2007. Mathematical biology: I. An introduction. Springer Science & Business Media.
32. MR Nahon. 2001. Phase evaluation and segmentation.
33. R Nevanlinna. 1970. The First Main Theorem in the Theory of Meromorphic Functions. Analytic Functions. 162-180.
34. A Nuttall, E Bedrosian. 1966. On the quadrature approximation to the Hilbert transform of modulated signals. Proceedings of the IEEE. 54 (10): 1458-1459.
35. AV Oppenheim. 1999. Discrete-time signal processing. Pearson Education India.
36. M Peltola. 2012. Role of editing of RR intervals in the analysis of heart rate variability. Frontiers in physiology. 3: 148.
37. B Picinbono. 1997. On instantaneous amplitude and phase of signals. IEEE Transactions on signal processing. 45 (3): 552-560.
38. AS Pikovsky, MG Rosenblum, GV Osipov, J Kurths. 1997. Phase synchronization of chaotic oscillators by external driving. Physica D: Nonlinear Phenomena. 104 (3-4): 219-238.
39. T Qian. 2010. Intrinsic mono-component decomposition of functions: an advance of Fourier theory. Mathematical Methods in the Applied Sciences. 33 (7): 880-891.
40. A Rihaczek, E Bedrosian. 1966. Hilbert transforms and the complex representation of real signals. Proceedings of the IEEE. 54 (3): 434-435.

41. MG Rosenblum, L Cimponeriu, A Bezerianos, A Patzak, R Mrowka. 2002. Identification of coupling direction: application to cardiorespiratory interaction. Physical Review E. 65 (4): 041909.
42. MG Rosenblum, AS Pikovsky. 2001. Detecting direction of coupling in interacting oscillators. Physical Review E. **64** (4): 045202.
43. C Schäfer, MG Rosenblum, HH Abel, J Kurths. 1999. Synchronization in the human cardiorespiratory system. Physical Review E. **60** (1): 857.
44. C Schäfer, MG Rosenblum, J Kurths, HH Abel. 1998. Heartbeat synchronized with ventilation. nature. 392 (6673): 239-240.
45. KH Shelley. 2007. Photoplethysmography: beyond the calculation of arterial oxygen saturation and heart rate. Anesthesia & Analgesia. 105 (6): S31-S36.
46. M Sourisseau, HT Wu, Z Zhou. 2019. Inference of synchrosqueezing transform--toward a unified statistical analysis of nonlinear-type time-frequency analysis. arXiv preprint arXiv:1904.09534.
47. D Vakman. 1972. On the definition of concepts of amplitude, phase and instantaneous frequency of a signal. Radio Eng Electron Phys. 17 (5): 754-759.
48. D Vakman. 1996. On the analytic signal, the Teager-Kaiser energy algorithm, and other methods for defining amplitude and frequency. IEEE Transactions on signal processing. **44** (4): 791-797.
49. B Van der Pol B. 1946. The fundamental principles of frequency modulation. Journal of the Institution of Electrical Engineers-Part III: Radio and Communication Engineering. **93** (23): 153-158.
50. T Wigren. 2015. Model order and identifiability of non-linear biological systems in stable oscillation. IEEE/ACM transactions on computational biology and bioinformatics. **12** (6): 1479-1484.
51. HT Wu. 2011. Adaptive analysis of complex data sets. Princeton University.
52. HT Wu. 2013. Instantaneous frequency and wave shape functions (I). Applied and Computational Harmonic Analysis. 35 (2): 181-199.
53. HT Wu. 2020. "Current state of nonlinear-type time-frequency analysis and applications to high-frequency biomedical signals." Current Opinion in Systems Biology.
54. HT Wu, A Alian, K Shelley. 2020. A new approach to complicated and noisy physiological waveforms analysis: peripheral venous pressure waveform as an example. Journal of Clinical Monitoring and Computing: 1-17.

Table 1 Phase shift and phase agreement among five algorithms and three respiratory signals

		Phase shift	p-value	Phase agreement	p-value
Flow VS Impe	BPF-HT	1.37±0.30	0.81	0.49±0.16	<0.00001*
	BKD	1.30±0.27	0.58	0.60±0.18	<0.00001*
	CWT-fixed	1.31±0.27	0.74	0.46±0.27	<0.00001*
	CWT-tvBPF	1.31±0.27	0.94	0.25±0.17	0.0006*
	SST	1.32±0.27	-	0.20±0.22	-
Flow VS $ETCO_2$	BPF-HT	-2.12±0.16	0.14	0.97±0.25	<0.00001*
	BKD	-2.15±0.16	0.53	0.83±0.38	<0.00001*
	CWT-fixed	-2.15±0.15	0.56	0.65±0.46	<0.00001*
	CWT-tvBPF	-2.17±0.16	0.94	0.37±0.37	0.0006*
	SST	-2.17±0.16	-	0.28±0.43	-
Impe VS $ETCO_2$	BPF-HT	1.62±1.70	<0.001*	2.16±0.55	<0.00001*
	BKD	2.25±1.34	0.02	1.67±0.81	<0.00001*
	CWT-fixed	2.12±1.42	0.003*	1.54±0.98	<0.00001*
	CWT-tvBPF	2.34±1.39	0.91	0.91±0.89	0.21
	SST	2.32±1.45	-	0.80±0.88	-

p value was evaluated as Mann-Whitney Wilcoxon test when comparing with SST. *: statistically significant with the level 0.05 corrected by the Bonferroni correction. Abbreviation: Impe: Impedance; ETCO2: End tidal CO2; BPF-HT: Hilbert transform followed by a bandpass filter; CWT-fixed: Continuous wavelet transform with a fixed spectral band; CWT-tvBPF: Continuous wavelet transform with a time varying bandpass filter; SST: Synchrosqueezing transform.

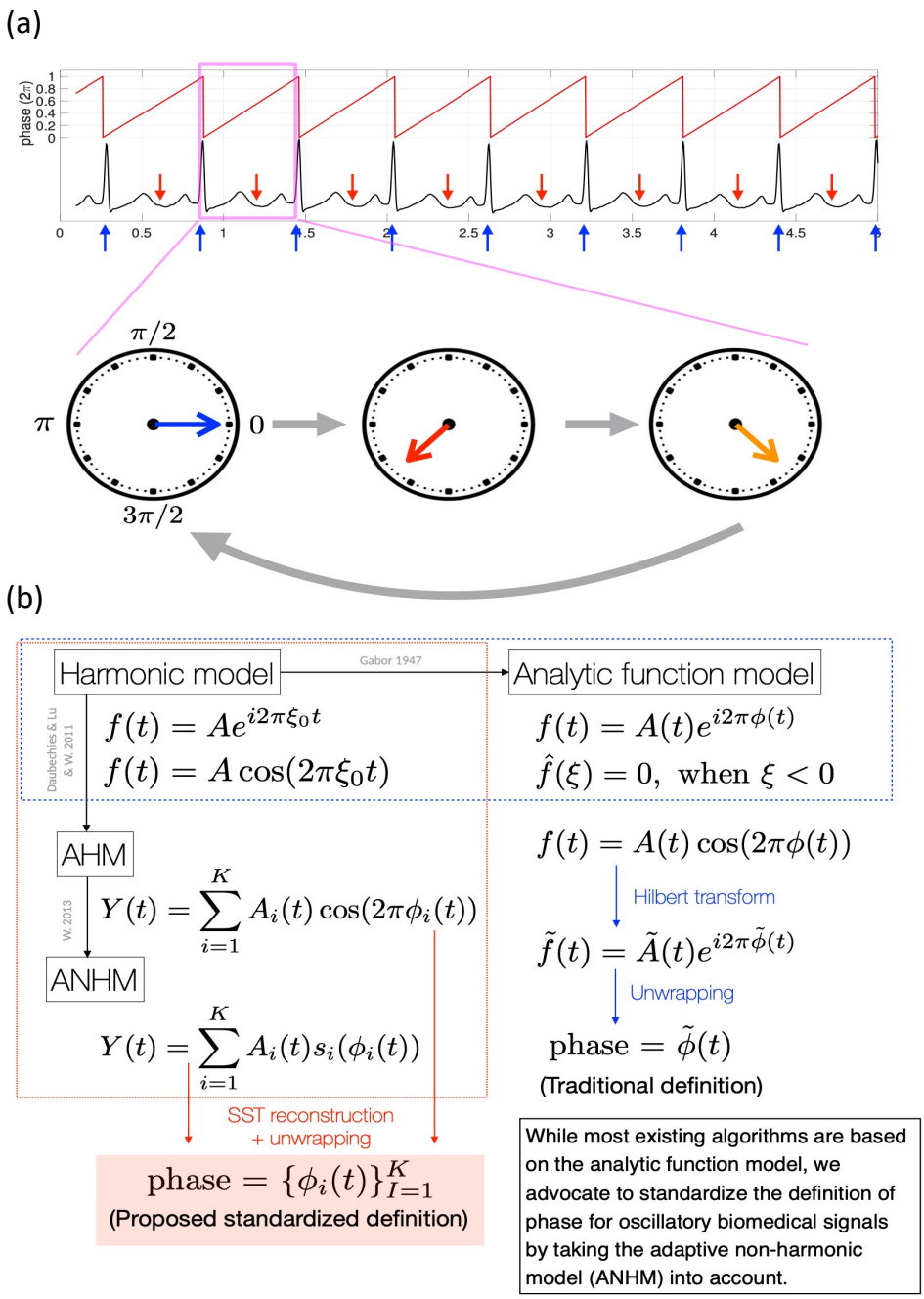

Figure 1: (a) The red curve on the top is the phase function associated with the ECG shown in the black curve, which ranges from 0 to 1 with the unit 2π. The cycle indicated by the magenta box is zoomed in to illustrate the idea of phase with a clock-like circling plot, where the time flow is indicated by the gray arrows. The blue arrows below the ECG signal indicate the status associated the phase 0, and the red arrows above the ECG signal indicate the status associated with the phase $5\pi/4$. The phase 0 is associated with the R peaks, and the phase $5\pi/4$ is associated with the T end. In our proposed standardization, the phase is defined as a monotonically increasing function. This might cause some confusions in the illustrated phase in

the red curve. Since the phase is the argument (or the angle) of the complex value, a phase value θ is not different from a phase value $\theta + 2k\pi$ for any integer k. Therefore, one way to plot the phase function is plotting the residue of the phase function by finding its value modulo 2π.

(b) A summary of models for the definition of phase function. The traditional phase is shown on the right-hand side, and the proposed standardized phase is shown on the left-hand side.

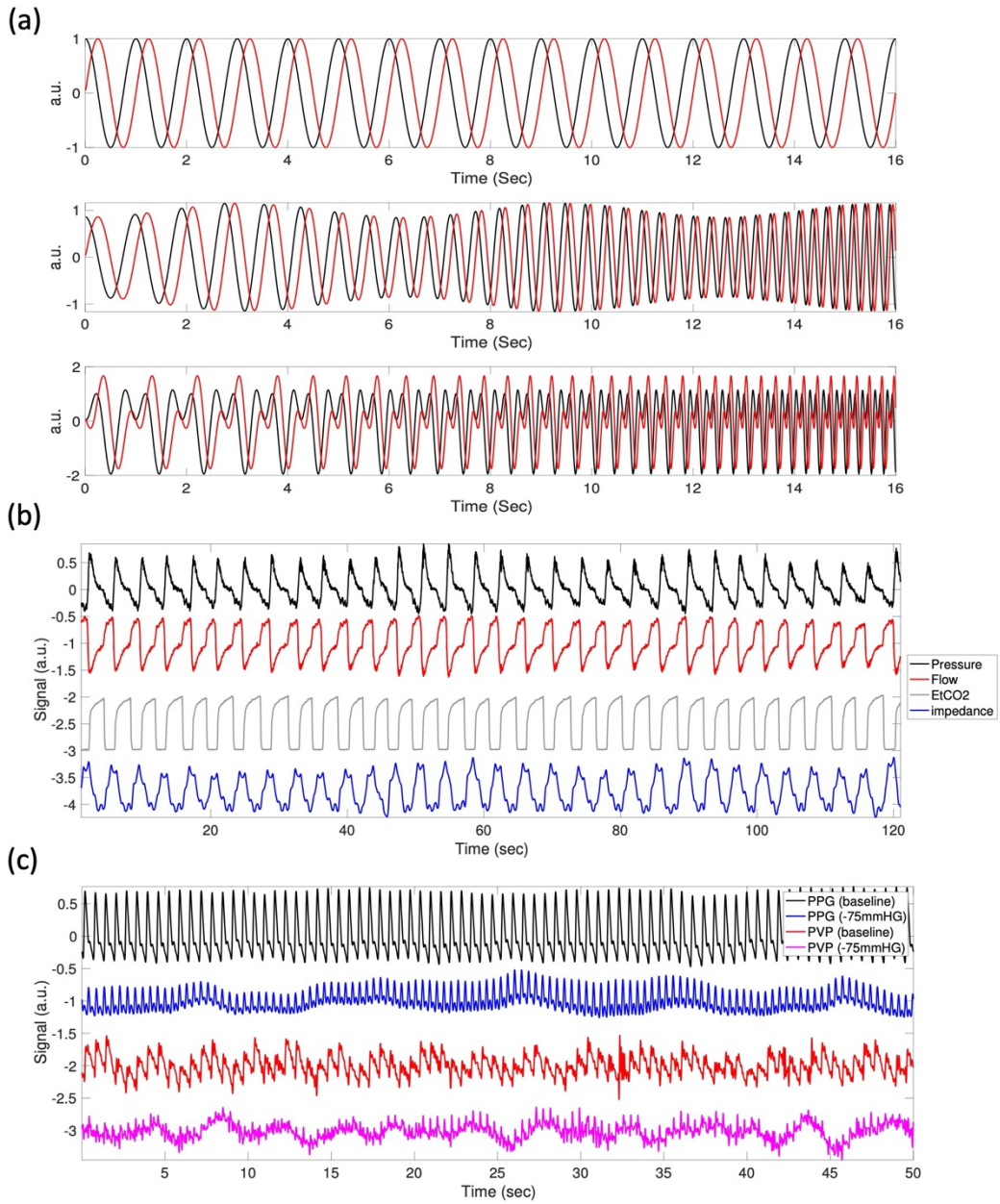

Figure 2: (a) illustration of simulated signals satisfying different models. Top: the harmonic model in equation (1) $f(t) = e^{i2\pi t}$; middle: the adaptive harmonic model in equation (3) $f(t) = (1 + 0.3\cos(t))\, e^{i2\pi(t+0.02t^{2.5})}$; bottom: the wave-shape model in equation (5) with $L = 1$, $f(t) = e^{i2\pi(t+0.02t^{2.5})} + 0.95e^{i[4\pi(t+0.02t^{2.5})+3]}$. The black and red curves are the real and imaginary parts of the complex form, respectively. (b) An illustration of various respiratory signals recorded simultaneously. The morphologies of those respiratory signals are different, and this difference is mainly encoded in the multiples. (c) An illustration of photoplethymogram (PPG) and peripheral venous pressure (PVP) signals recorded simultaneously during the lower body negative pressure (LBNP) experiment. The four signals from top to bottom are the PPG signal

during the baseline, the PPG signal during the -75 mmHg negative pressure, the PVP signal during the baseline, and the PVP signal during the -75 mmHg negative pressure. The morphologies of the same channels are different during different physiological status, and this difference is mainly encoded in the multiples.

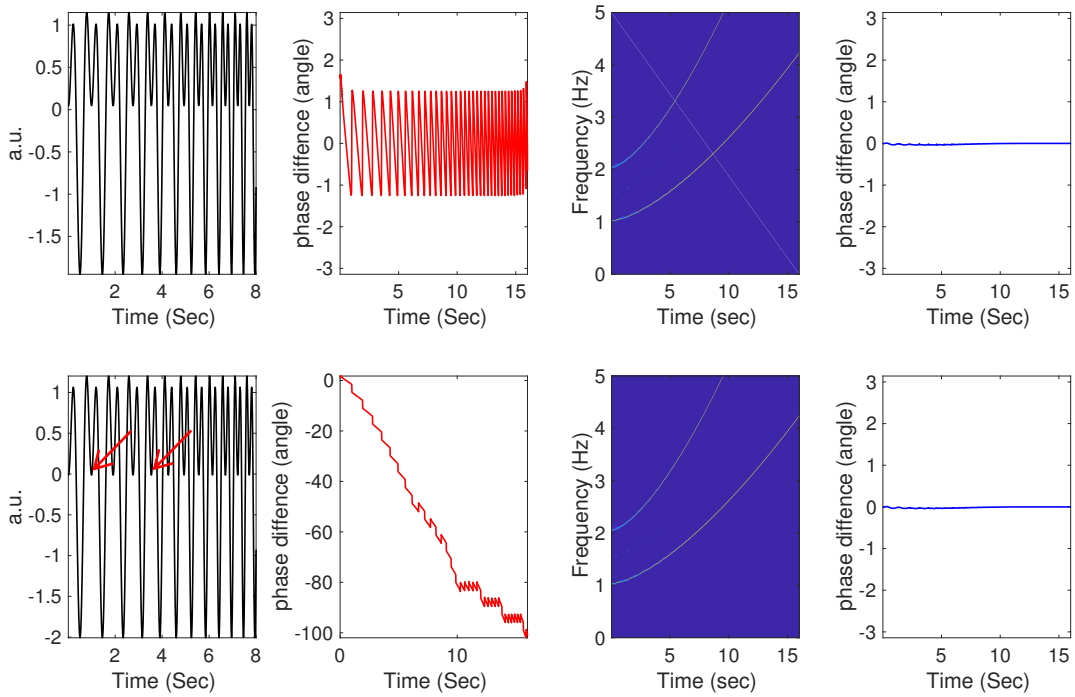

Figure 3: An illustration of the potential problem the Hilbert transform might encounter. The first signal, the real part of $f_1(t) = e^{i2\pi(t+0.02t^{2.5})} + 0.95e^{i[4\pi(t+0.02t^{2.5})+3]}$, is shown on the left top panel, and the second signal, the real part of $f_2(t) = e^{i2\pi(t+0.02t^{2.5})} + 1.01e^{i[4\pi(t+0.02t^{2.5})+3]}$ is shown on the left bottom panel. Note that the smaller trough of the real part of $f_2(t)$ crosses zero since the first harmonic has a larger amplitude than the fundamental component (red arrows). In the left middle columns, the red lines are the difference of the phase of the fundamental component, $\varphi(t) = 2\pi(t + 0.02t^{2.5})$, and the estimated phase $\tilde{\varphi}(t)$ by directly applying the Hilbert transform. It is clear that for $f_1(t)$, there is an obvious zig-zag difference between the estimated phase function $\tilde{\varphi}(t)$ and the proposed phase function $\varphi(t)$. However, for $f_2(t)$, there is an obvious cumulative phase estimation error as time evolves. This comes from the winding number issue due to the larger amplitude of the first harmonic. Due to the frequency modulation, the bandpass filter or continuous wavelet transform does not work as well (results not shown). In the right middle columns, the time-frequency representations of $f_1(t)$ and $f_2(t)$ determined by the synchrosqueezing transform (SST) are shown. In the right column, the blue lines are the difference of the estimated phase by SST and the proposed phase function $\varphi(t)$. Despite the winding issue, SST provides a consistent phase estimation.

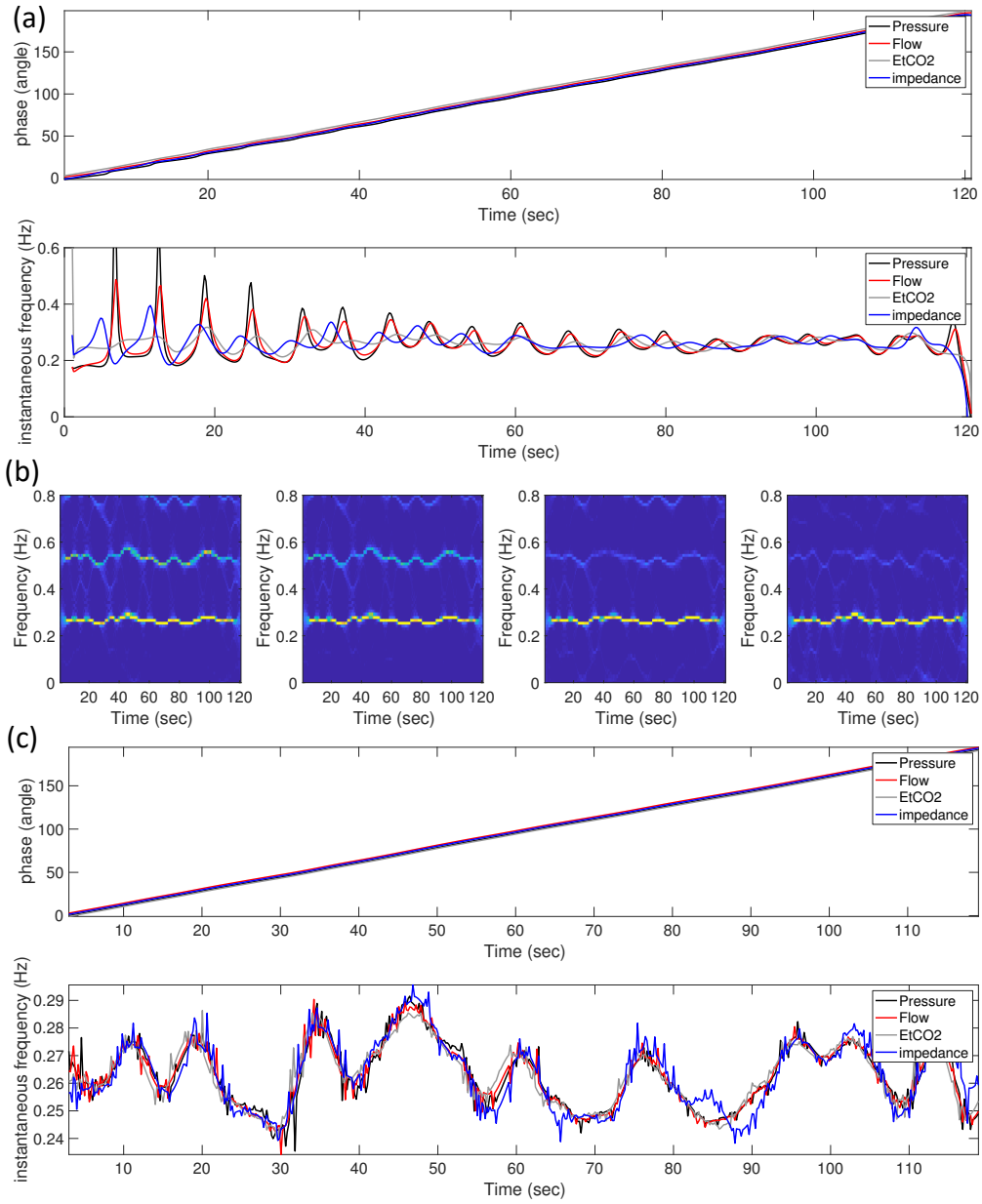

Figure 4: (a) An example of determining phases of various respiratory signals by the Hilbert transform followed by the band-pass filter (BPF-HT), where the band is 0.1-0.4 Hz determined by the dominant respiratory frequency. The phases, and hence their derivatives, are not consistent from one sensor to another. More importantly, while the definition of instantaneous frequency is mathematically correct, physiologically it is not sensible. The result by the continuous wavelet transform with a fixed spectral band (CWT-fixed) is similar and not shown. (b) An example of determining phases of various respiratory signals by the synchrosqueezing transform (SST). From left to right: the time-frequency representations of the pressure, flow, end-tidal CO_2, and impedance signals determined by SST. (c) Top panel: the phases of four respiratory signals estimated by SST. Bottom panel: the instantaneous frequency of four respiratory signals. The respiratory phases estimated from different sensors are more consistent, except a global phase shift. Also, the derivatives, which is the instantaneous

frequency by our definition, are consistent. The results by CWT with a time-varying spectral band (CWT-tvBPF) is similar and is not shown.

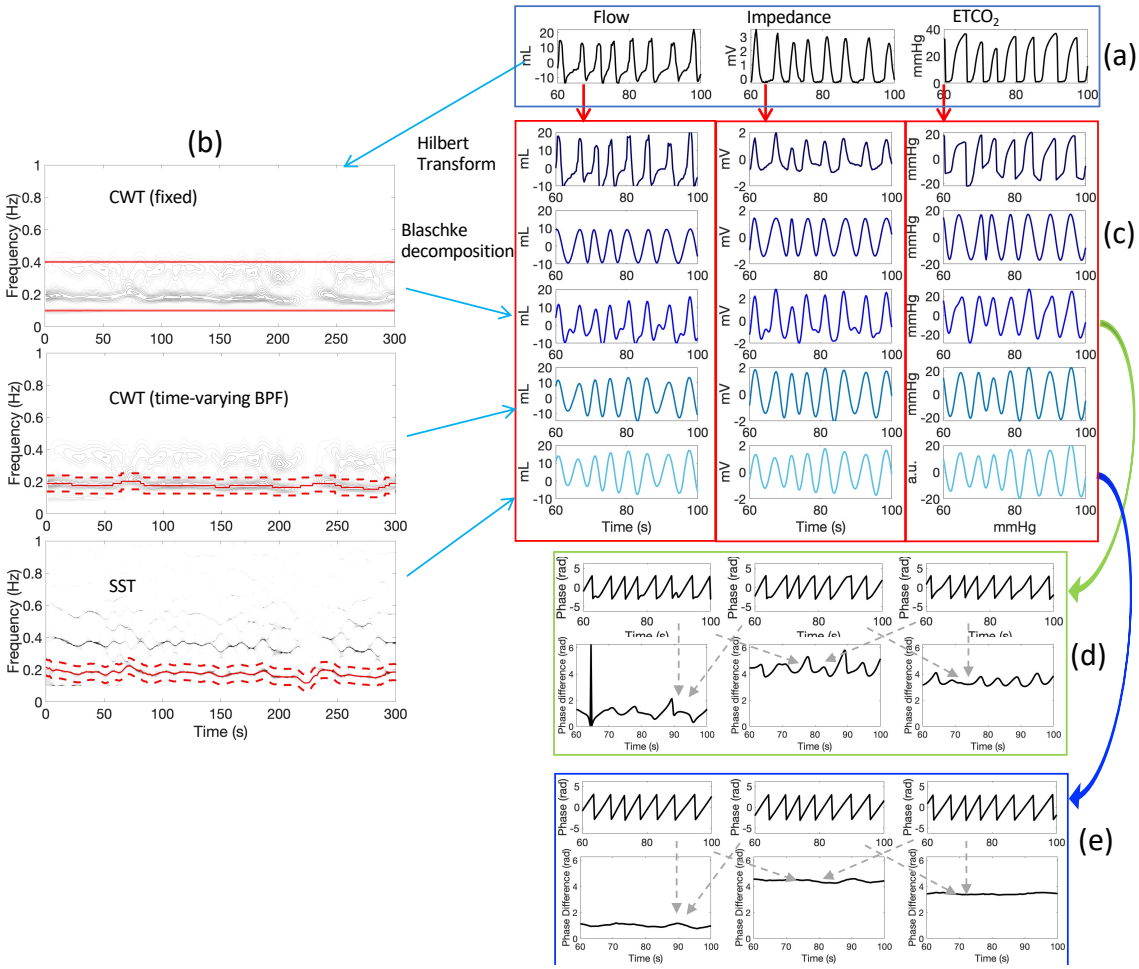

Figure 5: A comparison of different phase reconstruction methods from different respiratory sensors. (a) Three different respiratory signals. (b) The time-frequency representation (TFR) of the flow, impedance and end-tidal CO_2 ($EtCO_2$) signals, which were determined by CWT (top and middle) and SST (bottom) respectively. The fixed spectral band for CWT (CWT-fixed) reconstruction is shown in the top subfigure as red lines. The time-varying spectral bands for CWT and SST are plotted as dashed red curves above and below the solid red curve indicating the instantaneous frequency in the middle and bottom plots. (c) The reconstructed fundamental component by different methods. Each column is associated with one signal, and each row is associated with one method. (d) The phase estimated by CWT with a fixed spectral band mod by π is shown in the top row, where the phases are different. The phase difference between two phases estimated from two sensors is shown in the bottom row. (e) Same as (d), but the phase is estimated by SST. It is obvious that the fluctuation is less compared with the CWT-fixed method. The phase estimated by CWT with the time-varying bandpass filter is similar (not shown).

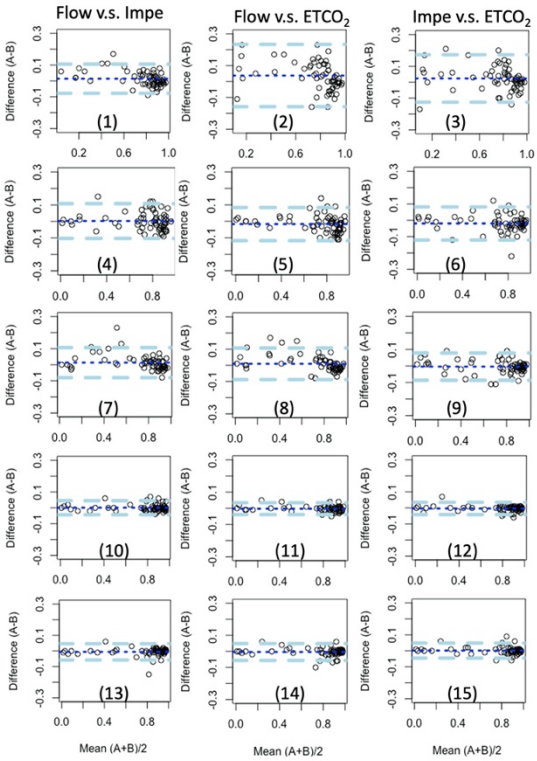

Algorithm	Sensors comparison	Bias	Upper 95% agreement bound [95%CI]	Lower 95% agreement bound [95%CI]
BPF-HT	(1) Flow VS Impe	0.01	0.11 [0.09, 0.13]	-0.08 [-0.06, -0.10]
	(2) Flow VS $ETCO_2$	0.04	0.23 [0.19, 0.28]	-0.16 [-0.11, -0.20]
	(3) Impe VS $ETCO_2$	0.02	0.17 [0.14, 0.21]	-0.13 [-0.09, -0.16]
BKD	(4) Flow VS Impe	0.003	0.11 [0.08, 0.13]	-0.10 [-0.08, -0.13]
	(5) Flow VS $ETCO_2$	-0.02	0.08 [0.06, 0.11]	-0.12 [-0.10, -0.14]
	(6) Impe VS $ETCO_2$	-0.02	0.08 [0.06, 0.11]	-0.12 [-0.10, -0.14]
CWT-fixed	(7) Flow VS Impe	0.13	0.11 [0.09, 0.13]	-0.08 [-0.06, -0.10]
	(8) Flow VS $ETCO_2$	0.01	0.11 [0.09, 0.13]	-0.09 [-0.07, -0.11]
	(9) Impe VS ETCO2	-0.004	0.08 [0.06, 0.10]	-0.09 [-0.07, -0.10]
CWT-tvBPF	(10) Flow VS Impe	0.0003	0.04 [0.04, 0.05]	-0.04 [-0.03, -0.05]
	(11) Flow VS $ETCO_2$	-0.003	0.03 [0.02, 0.04]	-0.04 [-0.03, -0.05]
	(12) Impe VS $ETCO_2$	-0.003	0.04 [0.03, 0.04]	-0.04 [-0.03, -0.05]
SST	(13) Flow VS Impe	-0.0005	0.04 [0.03, 0.05]	-0.05 [-0.04, -0.06]
	(14) Flow VS $ETCO_2$	-0.004	0.04 [0.04, 0.06]	-0.05 [-0.04, -0.06]
	(15) Impe VS $ETCO_2$	0.002	0.04 [0.04, 0.06]	-0.04 [-0.03, -0.06]

Abbreviation: Impe: Impedance; $ETCO_2$: End tidal CO_2; BPF-HT: Hilbert transform followed by a bandpass filter; BKD: Blaschke Decomposition; CWT-fixed: Continuous wavelet transform with a fixed spectral band; CWT-tvBPF: Continuous wavelet transform with a time varying bandpass filter; SST: Synchrosqueezing transform; CI: confidence interval.

Figure 6: Bland-Altman (BA) plot of the cardiopulmonary coupling index determined from different phase reconstruction methods and different respiratory signals. From left to right: the comparison of flow and impedance, the comparison of impedance and end-tidal CO_2 ($ETCO_2$), and the comparison of flow and $ETCO_2$. From top to bottom the phases of the respiratory signals are determined by the Hilbert transform followed by a bandpass filter (BPF-HT), the Blaschke decomposition, the continuous wavelet transform (CWT) with a fixed spectral band (CWT-fixed), the CWT with the proposed time-varying bandpass filter (CWT-tvBPF), and the synchrosqueezing transform (SST). The comparison is summarized in the table shown on the right-hand side, which suggests that the agreements of respiratory phases determined by CWT-tvBPF and SST are higher than other methods.

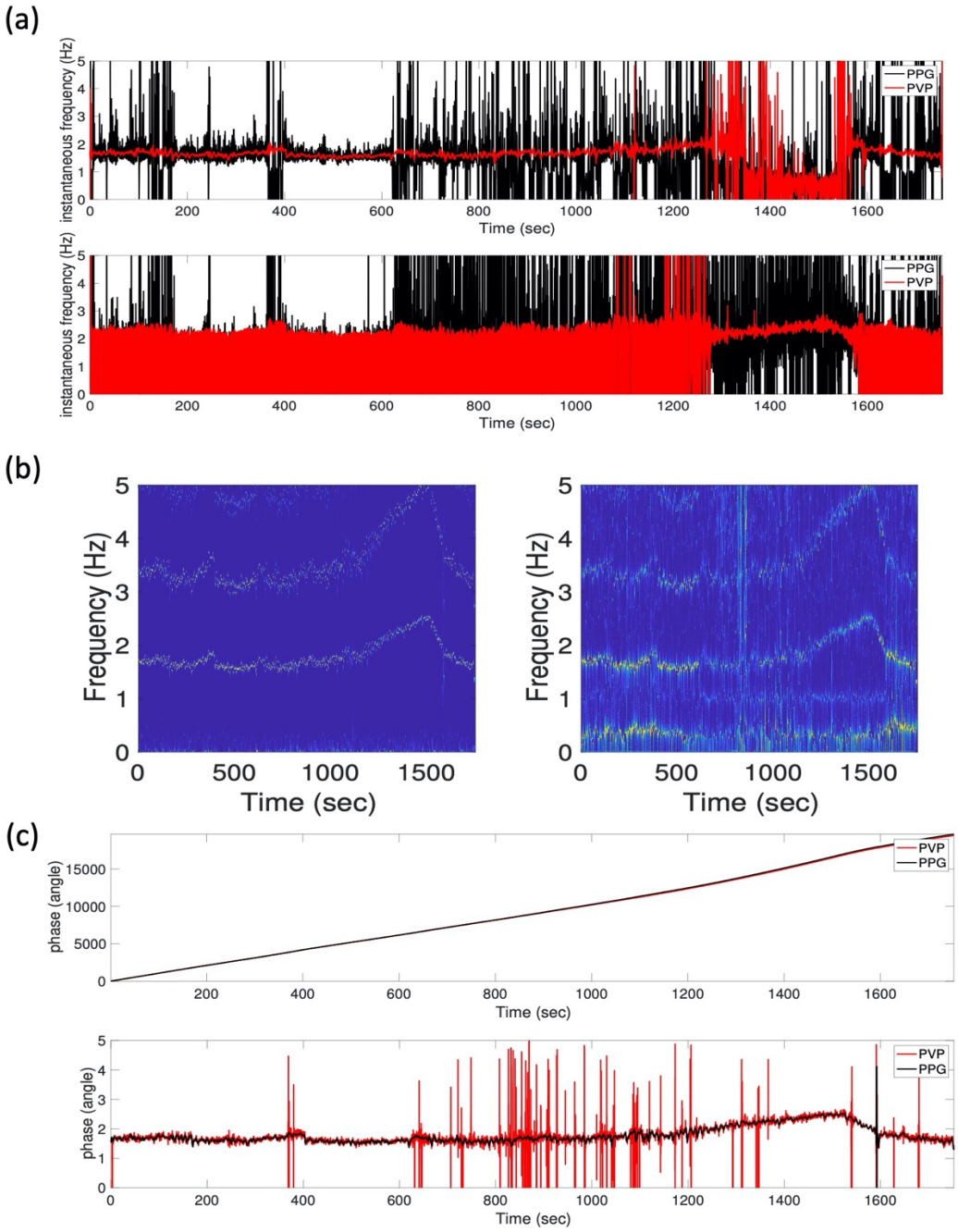

Figure 7: (a) An example of estimating phases of photoplethymogram (PPG) and peripheral venous pressure (PVP) signals by the Hilbert transform followed by a band-pass filter (BPF-HT) with different spectral bands, where the derivatives of the estimated phases, the instantaneous frequencies, are shown for a comparison. In the top panel, the spectral band is 0.5-2 Hz, while in the bottom panel, the spectral band is 0.5-4 Hz. The lower spectral bound 0.5 Hz is chosen to avoid the respiratory component impact, and the upper spectral bound 2 or 4 Hz is chosen to include sufficient cardiac information. However, in both cases, the phases, and hence their

derivatives, are not consistent between the PPG and PVP signals. The difference is clear over 1300-1600 second. This comes from the fact that the heart rate increases dramatically during 1300-1600 seconds during the lower body negative pressure experiment, and the chosen spectral bands, if fixed, may include insufficient fundamental component information or may be contaminated by its multiples. (b) An example of the time-frequency representations (TFRs) determined by the synchrosqueezing transform (SST). The TFR of the photoplethymogram (PPG) is shown on the left and the TFR of the peripheral venous pressure (PVP) is shown on the right. (c) the phases and the associated instantaneous frequency of the cardiac component in the PPG and PVP signals. The phases associated with the PPG and PVP signals are shown on the top, and the associated instantaneous frequency of the hemodynamic oscillation determined by differentiating the estimated phases are shown in the bottom. The phases of PPG and PVP signals are consistent. Also, the derivatives, which is the instantaneous frequency by our definition, are consistent, except some unwanted spikes in the PVP signal. This comes from the well-known fact that the PVP signal is usually too noisy to analyse with traditional tools.